

1      **Title:** MTL functional connectivity predicts stimulation-induced theta power

2  
3      **Authors:** E. A. Solomon<sup>1</sup>, R. Gross<sup>2</sup>, B. Lega<sup>3</sup>, M. R. Sperling<sup>4</sup>, G. Worrell<sup>5</sup>, S. A. Sheth<sup>6</sup>, K. A.  
4      Zaghloul<sup>7</sup>, B. C. Jobst<sup>8</sup>, J. M. Stein<sup>9</sup>, S. Das<sup>9</sup>, R. Gorniak<sup>10</sup>, C. Inman<sup>2</sup>, S. Seger<sup>3</sup>, J. E. Kragel<sup>11</sup>,  
5      D. S. Rizzuto<sup>11</sup>, M. J. Kahana<sup>11\*</sup>

6  
7      **Affiliations**

8      <sup>1</sup>University of Pennsylvania, Department of Bioengineering, Philadelphia, PA 19146

9      <sup>2</sup>Department of Neurosurgery, Emory School of Medicine, Atlanta, GA 30322

10      <sup>3</sup>Department of Neurosurgery, University of Texas Southwestern, Dallas, TX 75390

11      <sup>4</sup>Department of Neurology, Thomas Jefferson University Hospital, Philadelphia, PA 19107

12      <sup>5</sup>Department of Neurology, Department of Physiology and Bioengineering, Mayo Clinic,  
13      Rochester, MN 55905

14      <sup>6</sup>Department of Neurosurgery, Baylor College of Medicine, Houston, TX 77030

15      <sup>7</sup>Surgical Neurology Branch, National Institutes of Health, Bethesda, MD 20814

16      <sup>8</sup>Department of Neurology, Dartmouth Medical Center, Lebanon, NH 03756

17      <sup>9</sup>Department of Radiology, Hospital of the University of Pennsylvania, Philadelphia, PA 19104

18      <sup>10</sup>Department of Radiology, Thomas Jefferson University Hospital, Philadelphia, PA 19107

19      <sup>11</sup>University of Pennsylvania, Department of Psychology, Philadelphia, PA 19146

20  
21      \*Correspondence addressed to [kahana@psych.upenn.edu](mailto:kahana@psych.upenn.edu), [esolo@pennmedicine.upenn.edu](mailto:esolo@pennmedicine.upenn.edu)

22  
23      **Abstract/Summary**

24  
25      Focal electrical stimulation of the brain incites a cascade of neural activity that

26      propagates from the stimulated region to both nearby and remote areas, offering the potential to

27      control the activity of brain networks. Understanding how exogenous electrical signals perturb

28      such networks in humans is key to its clinical translation. To investigate this, we applied

29      electrical stimulation to subregions of the medial temporal lobe in 26 neurosurgical patients

30      fitted with indwelling electrodes. Networks of low-frequency (5-13 Hz) spectral coherence

31      predicted stimulation-evoked changes in theta (5-8 Hz) power, but only when stimulation was

32      applied in or adjacent to white matter. Furthermore, these power changes aligned with control-

33      theoretic predictions of how exogenous stimulation flows through complex networks, such as a

34      dispersal of induced activity when functional hubs are targeted. Our results demonstrate that

35 functional connectivity is predictive of causal changes in the brain, but that access to structural  
36 connections is necessary to observe such effects.

37

38 **Introduction**

39  
40 Intracranial brain stimulation is increasingly used to study disorders of human behavior  
41 and cognition, but very little is known about how these stimulation events affect neural activity.  
42 Though several recent studies have demonstrated the ability to modulate human memory with  
43 direct electrical stimulation (DES) of the cortex <sup>1-7</sup>, none have described the mechanism by  
44 which stimulation yields altered cognitive states. However, understanding how the brain  
45 responds to these exogenous currents is necessary to ultimately develop therapeutic interventions  
46 that rely on DES <sup>8,9</sup>.

47 Because it is often not possible to directly stimulate a given brain region of interest in  
48 clinical populations of neurosurgical volunteers, recent investigations have asked whether the  
49 brain's intrinsic functional or anatomical architecture can predict how mesoscale stimulation  
50 events propagate through the brain. In monkeys, Logothetis, et al. (2010) demonstrated that the  
51 effects of electrical stimulation propagated through known anatomical connections in the visual  
52 system. In humans, corticocortical evoked potentials (CCEPs), measured with intracranial EEG,  
53 have also been shown to propagate through anatomical and functional connections  
54 <sup>10,11</sup>, as has the fMRI BOLD response to stimulation <sup>12</sup>. These studies provide powerful evidence  
55 that the effects of stimulation are determined by the connectivity profile of a targeted region.  
56 More broadly, renewed interest in the idea of the brain as a controllable network <sup>13-15</sup> raises a  
57 testable hypothesis in need of empirical validation: to what extent does a brain's network  
58 architecture predict the cascade of physiologic change that accompanies a stimulation event?

59 In this study, we asked whether the functional connectivity of a stimulated region predicts  
60 where we observe changes in neural activity. To expand on prior work that has examined  
61 network architecture and stimulation, we adopted a paradigm that (1) measures stimulation's  
62 effect on low-frequency (theta) power, a cognitively-relevant electrophysiological biomarker,  
63 and (2) simultaneously considers the structural and functional connectivity of a targeted region.  
64 In 26 neurosurgical patients with indwelling electrodes, we stimulated different regions of the  
65 medial temporal lobe (MTL) and asked whether functional connectivity predicted modulations of  
66 theta power in distributed cortical regions. We showed that functional connectivity was only  
67 predictive of theta modulation when stimulation occurred in or near a white matter tract, but in  
68 those cases, stimulation could evoke sustained increases in theta power even in distant regions.  
69 Furthermore, functional networks only had such predictive power at low frequencies, in the theta  
70 and alpha bands (5-13 Hz).

71

## 72 **Results**

### 73 **Calculating a theta modulation index**

74 To determine how direct cortical stimulation propagates through brain networks, we  
75 collected intracranial EEG (iEEG) data from 26 patients undergoing clinical monitoring for  
76 seizures. Subjects rested passively in their hospital bed while we applied bipolar macroelectrode  
77 stimulation at varying frequencies (10-200 Hz) and amplitudes (0.25 to 1.5 mA) to MTL depth  
78 electrodes (see online Methods for details). Rectangular stimulation pulses were delivered for  
79 500 ms, followed by a 3-second inter-stimulation interval (Figure 1A-C). Each subject received  
80 at least 240 stimulation events ("trials") at 1-8 distinct sites in MTL gray or white matter (mean  
81 2.7 sites; see Supplementary Table 2 for stimulation locations). During a separate recording

82 session in which no stimulation occurred, for each subject we computed resting networks of low-  
83 frequency (5-13 Hz) coherence, motivated by prior literature that shows robust iEEG functional  
84 connectivity at low frequencies <sup>16-19</sup>. These networks reflect correlated low-frequency activity  
85 between all possible pairs of electrodes in a subject, during a period when subjects are passively  
86 waiting for a task to begin (Figure 2A).

87 For each stimulation trial, we computed theta power (5-8 Hz) in 900 ms windows before  
88 and after each 500 ms stimulation event, and compared the pre- vs. post-stimulation power  
89 across all trials with a paired *t*-test (Figure 1D). Next, we used linear regression to correlate the  
90 strength of a stimulation site’s network connectivity to a recording electrode with the power *t*-  
91 statistic at that electrode (Figure 2A-D). We included absolute distance as a factor in our  
92 regression, to only consider how connectivity relates to stimulation beyond the brain’s tendency  
93 to densely connect nearby regions <sup>20</sup>. The result is a model coefficient that indicates, independent  
94 of distance, the degree to which functional connectivity predicts stimulation-induced change in  
95 theta power at a recording site. The regression was repeated using permuted connectivity/evoked  
96 power relationships to generate a null distribution of model coefficients against which the true  
97 coefficient is compared. We refer to the resulting z-score as the “theta modulation index,” or  
98 TMI. High TMIs indicate functional network connectivity predicts observable stimulation-  
99 related change in theta power at distant sites.

100 **TMI is correlated with proximity to white matter**

101 At a group level of stimulation sites, TMI was significantly greater than zero (1-sample *t*-  
102 test,  $t(71) = 4.0, P = 0.0002$ ; Figure 3A), indicating that stimulation in the MTL tends to evoke  
103 network-driven change in theta power in distant regions. However, we noted substantial  
104 heterogeneity between stimulation sites, with some showing little or no ability to modulate

105 network-wide theta activity, as reflected by TMIs near zero. To explain this heterogeneity, we  
106 hypothesized that, as earlier work demonstrated<sup>11,21,22</sup>, structural connections (i.e. white matter  
107 tracts) may be key to the propagation of electrical stimulation throughout the brain.

108 To test whether structural connections play a role in stimulation propagation, we asked  
109 whether TMI was correlated with the proximity of a stimulation site to white matter. If these  
110 measures are correlated, it would indicate that functional connectivity is predictive of physiology  
111 only insofar as white matter tracts are accessible. We binned stimulation sites according to  
112 whether they were placed in gray matter (n = 32, lower 50<sup>th</sup> percentile of distances to white  
113 matter), near white matter (n = 33, upper 50<sup>th</sup> percentile of distances to white matter), or within  
114 white matter (n = 7, manually identified by a neuroradiologist; Figure 3A; see Supplementary  
115 Figure 1 for anatomical placement of each white matter target). We found that TMI was  
116 significantly increasing with white matter placement, relative to a permuted distribution  
117 (permuted  $P < 0.001$ ; Figure 3B). The TMI for gray matter sites was not significantly different  
118 than zero (1-sample  $t$ -test,  $t(31) = 1.4$ ,  $P = 0.18$ ), while TMI for sites near or in white matter was  
119 significant ( $P < 0.05$ ). This relationship holds in a Pearson correlation agnostic to any electrode  
120 categorization ( $r = 0.33$ ,  $P = 0.005$ ; Supplementary Figure 2). This finding does not mean gray  
121 matter stimulation fails to induce theta activity, but it does suggest gray matter stimulation may  
122 result in theta activity that is uncorrelated with functional connectivity to remote sites.

123 Taken together, these results show that direct electrical stimulation of the MTL can  
124 induce spectral power changes across a distributed network of regions, particularly if stimulation  
125 occurs in or proximal to white matter. When this occurred, we discovered that functional low-  
126 frequency coherence is predictive of where stimulation-related modulations in theta power are  
127 observed.

128 **Network properties of MTL stimulation**

129 Having shown that stimulation in or near white matter sites induces distributed changes  
130 in theta power, we next sought to characterize the directionality of change. Specifically, high  
131 TMIs could be caused by increases in theta power at electrodes with strong functional  
132 connectivity to the stimulation target, or decreases in theta power at electrodes with weak  
133 connectivity to the stimulation target. To distinguish between these possibilities, we further  
134 examined theta power changes in detail among the 16 stimulation sites that exhibited significant  
135 ( $P < 0.05$ ) TMI (see Supplementary Table 1 for statistics and anatomical placement of each  
136 significant site). In this subset, we measured the average pre- vs. post-stimulation theta power at  
137 the five electrodes with the strongest functional connectivity to the stimulation site (controlled  
138 for distance), and the five electrodes with the weakest functional connectivity. At strongly-  
139 connected sites, theta power change was significantly positive (1-sample  $t$ -test,  $t(15) = 5.6$ ,  $P =$   
140  $4.0 \times 10^{-5}$ ) and significantly greater than power change at weakly-connected sites (paired  $t$ -test,  
141  $t(15) = 6.03$ ,  $P = 1.7 \times 10^{-5}$ ; Figure 4B). No significant power change was observed at sites with  
142 weak functional connectivity (1-sample  $t$ -test,  $t(15) = 1.5$ ,  $P = 0.15$ ). Notably, we observed that  
143 of the 16 significant sites analyzed here, 15 were placed in or near white matter. We conclude  
144 that stimulation causes increased theta power at strongly-connected sites and little to no change  
145 in power at weakly-connected sites.

146 Principles of network control theory suggest a relation between the connectivity profile –  
147 or network topology – of a stimulation site and the ensuing change in brain activity. Network  
148 “hubs,” or regions with strong connectivity to the rest of the brain, are generally less capable of  
149 modulating the brain’s overall state versus non-hubs, or regions with strong connections to only  
150 a few areas<sup>14,23</sup>. To directly test this hypothesis, we asked whether stimulation-induced theta

151 power correlated with the functional “hubness” of a stimulation site. We again took our measure  
152 of stimulation-induced activity to be the theta power change at the 5 recording sites with the  
153 strongest functional connectivity to the stimulation site, and tested this metric against the node  
154 strength of a stimulation site, an indicator of hubness (for this analysis, we considered all  
155 stimulation sites in or near white matter;  $n = 40$ ). When weak hubs (lower tercile of hub scores;  $n$   
156 = 13) were stimulated, power change at connected recording sites was significantly greater than  
157 zero (1-sample t-test,  $t(12) = 3.6$ ,  $P = 0.003$ ), but stimulation at strong hubs (upper tercile;  $n =$   
158 14) evoked no significant power modulation ( $t(13) = 0.15$ ,  $P = 0.87$ ; Figure 4D). While  
159 counterintuitive, this result is in line with the prediction of network control theory; stimulation at  
160 a site with many connections may disperse the effect of perturbation, yielding lesser activation in  
161 downstream regions.

162 Our choice of low-frequency (5-13 Hz) functional connectivity as the basis for predicting  
163 distributed changes in theta power was motivated by prior studies that have shown strong,  
164 cognitively-relevant connectivity at low frequencies particularly the theta and alpha bands <sup>16,17,19</sup>.  
165 However, others have noted significant inter-regional connectivity in the beta and gamma bands  
166 <sup>24</sup>. As our study presented a unique opportunity to examine the causal nature of functional  
167 connectivity, we asked whether functional connectivity in other frequency bands is also  
168 predictive of downstream power modulations. Among all MTL electrodes placed in or near white  
169 matter ( $n = 40$ ), we asked whether TMI was significant for networks constructed from any  
170 frequency to a maximum of 50 Hz. No frequencies outside the alpha/theta bands exhibited  
171 significant group-level TMIs, after correction for multiple comparisons ( $P < 0.05$ , Benjamini-  
172 Hochberg correction; Figure 4E). This demonstrates that functional networks constructed from  
173 high frequencies ( $> 13$  Hz) are not predictive of stimulation-induced theta activity.

174

175 **Discussion**

176        We set out to test a fundamentally simple hypothesis: Do functional connections in the  
177    brain predict how focal electrical stimulation flows from one region to another? Though critical  
178    to the future of brain stimulation and therapeutic development, this hypothesis has not seen  
179    rigorous testing. Prior studies indicate that connectivity plays a role in how stimulation events  
180    perturb distant brain regions <sup>10,12,21,22</sup>, but fundamental assumptions of graph-theoretic models  
181    remain untested <sup>13</sup>. More broadly, no prior studies have addressed whether iEEG-based  
182    functional connectivity indicates anything about causal relationships in the brain, or whether it is merely  
183    a correlative measure. In this manuscript, we specifically tested a hypothesis about the  
184    effects of stimulation on theta power, given an especially rich literature showing the cognitive  
185    relevance of theta oscillations <sup>25–28</sup>. This theoretically-motivated choice also served to reduce the  
186    number of possible tests we could have run on other frequency bands implicated in cognition.

187        We discovered that (1) modulation of low-frequency power is correlated with functional  
188    connectivity, but only if stimulation occurred in or near white matter, (2) stronger functional  
189    connections yield greater power increases, (3) stimulation of strong functional hubs weakens  
190    downstream power changes, and (4) low-frequency functional connections are more strongly  
191    predictive of neural activity than high frequency connections. These results align with  
192    predictions offered by models of the brain as a dynamical system built on a white matter  
193    scaffold. Namely, stronger connections generally yield bigger evoked changes, but too many  
194    strong connections can dilute the effect of stimulation – perhaps by dispersing stimulation energy  
195    across many regions.

196                   The meaning of functional connectivity is a subject of considerable debate. Correlated  
197                   activity between two parts of the brain may reflect direct connection between the two, an indirect  
198                   connection through a third region, or the activity of a third region independently driving activity  
199                   in each <sup>29</sup>. Though most neuroscientists are aware of such limitations, functional connectivity is  
200                   often implicitly treated as a measure of causality nonetheless. Our use of targeted stimulation  
201                   allowed us to test whether this implicit assumption is true. Our results generally support the idea  
202                   that functional connectivity indicates causality; when stimulation occurs in or near white matter,  
203                   we could predict where power changes would occur based on distance-independent measures of  
204                   low-frequency functional connections. This finding aligns with observations that intrinsic  
205                   functional connectivity in MRI is constrained by white matter anatomy <sup>30</sup>. However, substantial  
206                   variance in power modulation remained unexplained by connectivity, and we also showed that  
207                   propagation of gray matter stimulation – still rich with functional connections – cannot be  
208                   predicted in the same way.

209                   This study faces several limitations. First, we only assessed stimulation in the MTL,  
210                   which has a distinct architecture that may affect how stimulation propagates to other regions –  
211                   the effects of stimulation at the cortical surface could differ markedly. High-resolution diffusion  
212                   tractography would be needed to make strong claims about which MTL white matter tracts are  
213                   accessed by stimulation. Second, though our hypothesis about theta was theoretically grounded,  
214                   this choice leaves open the question as to whether higher frequency activity is also affected by  
215                   stimulation – though theta power may be a useful measure of how stimulation alters neural  
216                   excitability <sup>31–33</sup>, changes in population spiking would be better captured by high-frequency  
217                   activity (e.g. > 60 Hz) <sup>34,35</sup>.

218            In this study we solely analyze stimulation through the lens of changes in brain  
219            physiology. However, with an eye towards the eventual therapeutic use of stimulation, the results  
220            here bridge prior studies of stimulation and behavior with underlying neural mechanisms. A  
221            recent study reported decreases in episodic memory performance during stimulation at certain  
222            times, associated with increases in cortical theta power <sup>3</sup>. Additionally, memory performance  
223            was noted to increase with theta-burst stimulation of the perforant path, a major white matter  
224            tract of the MTL <sup>4</sup>. Deep brain stimulation targeted to white matter tracts has also been shown to  
225            improve outcomes in treatment-resistant depression <sup>9</sup>. Collectively, these findings are supported  
226            by the results here – white matter stimulation appears to evoke remote increases in neural  
227            activity. Few studies have deeply examined stimulation-induced changes in physiology with  
228            behavioral enhancement, though our approach outlined here enables us to do exactly that in  
229            future work.

230            Here we demonstrated that functional connections in the human brain inform how  
231            stimulation evokes remote changes in neural activity. This is powerful new evidence that, even in  
232            the absence of knowledge about an individual's structural connectome, functional connectivity  
233            reflects causality in the brain – a finding with significant implications for how neuroscientists  
234            interpret inter-regional correlations of neural activity. Furthermore, by showing that stimulation-  
235            evoked changes interact with the functional hubness of a targeted site, we provided critical,  
236            empirical evidence that network control theory can model real-world brain dynamics.

237  
238  
239  
240  
241  
242  
243

244 **References**

245

246 1. Jacobs, J. *et al.* Direct Electrical Stimulation of the Human Entorhinal Region and  
247 Hippocampus Impairs Memory. *Neuron* **92**, 983–990 (2016).

248 2. Ezzyat, Y. *et al.* Closed-loop stimulation of temporal cortex rescues functional networks  
249 and improves memory. *Nat. Commun.* **9**, 365 (2018).

250 3. Ezzyat, Y. *et al.* Direct Brain Stimulation Modulates Encoding States and Memory  
251 Performance in Humans. *Curr. Biol.* **27**, 1251–1258 (2017).

252 4. Titiz, A. S. *et al.* Theta-burst microstimulation in the human entorhinal area improves  
253 memory specificity. *Elife* **6**, e29515 (2017).

254 5. Suthana, N. *et al.* Memory Enhancement and Deep-Brain Stimulation of the Entorhinal  
255 Area. *N. Engl. J. Med.* **366**, 502–510 (2012).

256 6. Inman, C. S. *et al.* Direct electrical stimulation of the amygdala enhances declarative  
257 memory in humans. *Proc. Natl. Acad. Sci.* 201714058 (2017).  
258 doi:10.1073/PNAS.1714058114

259 7. Hampson, R. E. *et al.* Developing a hippocampal neural prosthetic to facilitate human  
260 memory encoding and recall. *J. Neural Eng.* **15**, 36014 (2018).

261 8. Sreekumar, V., Wittig, J. H., Sheehan, T. C. & Zaghloul, K. A. Principled Approaches to  
262 Direct Brain Stimulation for Cognitive Enhancement. *Front. Neurosci.* **11**, 650 (2017).

263 9. Riva-Posse, P. *et al.* A connectomic approach for subcallosal cingulate deep brain  
264 stimulation surgery: prospective targeting in treatment-resistant depression. *Mol.*  
265 *Psychiatry* **23**, 843–849 (2018).

266 10. Keller, C. J. *et al.* Intrinsic functional architecture predicts electrically evoked responses in  
267 the human brain. *Proc. Natl. Acad. Sci. U. S. A.* **108**, 10308–13 (2011).

268 11. Matsumoto, R. *et al.* Functional connectivity in the human language system: a cortico-  
269 cortical evoked potential study. *Brain* **127**, 2316–2330 (2004).

270 12. Oya, H. *et al.* Mapping effective connectivity in the human brain with concurrent  
271 intracranial electrical stimulation and BOLD-fMRI. *J. Neurosci. Methods* **277**, 101–112  
272 (2017).

273 13. Gu, S. *et al.* Controllability of structural brain networks. *Nat. Commun.* **6**, 8414 (2015).

274 14. Muldoon, S. F. *et al.* Stimulation-Based Control of Dynamic Brain Networks. *PLOS*  
275 *Comput. Biol.* **12**, e1005076 (2016).

276 15. Kim, K., Ekstrom, A. D. & Tandon, N. A network approach for modulating memory  
277 processes via direct and indirect brain stimulation: Toward a causal approach for the  
278 neural basis of memory. *Neurobiol. Learn. Mem.* **134**, 162–177 (2016).

279 16. Solomon, E. A. *et al.* Widespread theta synchrony and high-frequency desynchronization  
280 underlies enhanced cognition. *Nat. Commun.* **8**, 1704 (2017).

281 17. Betzel, R. F. *et al.* Inter-regional ECoG correlations predicted by communication  
282 dynamics, geometry, and correlated gene expression. (2017).

283 18. Solomon, E. A. *et al.* Functional wiring of the human medial temporal lobe. *bioRxiv*  
284 257899 (2018). doi:10.1101/257899

285 19. Watrous, A. J., Tandon, N., Conner, C. R., Pieters, T. & Ekstrom, A. D. Frequency-  
286 specific network connectivity increases underlie accurate spatiotemporal memory  
287 retrieval. *Nat. Neurosci.* **16**, 349–56 (2013).

288 20. Honey, C. J. *et al.* Predicting human resting-state functional connectivity from structural  
289 connectivity. *Proc. Natl. Acad. Sci. U. S. A.* **106**, 2035–40 (2009).

290 21. Logothetis, N. K. *et al.* The effects of electrical microstimulation on cortical signal  
291 propagation. *Nat. Publ. Gr.* **13**, (2010).

292 22. Kubota, Y. *et al.* In vivo human hippocampal cingulate connectivity: A corticocortical  
293 evoked potentials (CCEPs) study. *Clin. Neurophysiol.* **124**, 1547–1556 (2013).

294 23. Medaglia, J. D., Pasqualetti, F., Hamilton, R. H., Thompson-Schill, S. L. & Bassett, D. S.  
295 *Brain and Cognitive Reserve: Translation via Network Control Theory.* (2016).

296 24. Fell, J. *et al.* Human memory formation is accompanied by rhinal-hippocampal coupling  
297 and decoupling. *Nat. Neurosci.* **4**, 1259–64 (2001).

298 25. Buzsáki, G. & Moser, E. I. Memory, navigation and theta rhythm in the hippocampal-  
299 entorhinal system. *Nat. Neurosci.* **16**, 130–138 (2013).

300 26. Rutishauser, U., Ross, I. B., Mamelak, A. N. & Schuman, E. M. Human memory strength  
301 is predicted by theta-frequency phase-locking of single neurons. *Nature* **464**, 903–907  
302 (2010).

303 27. Lega, B. C., Jacobs, J. & Kahana, M. Human hippocampal theta oscillations and the  
304 formation of episodic memories. *Hippocampus* **22**, 748–761 (2012).

305 28. Düzel, E., Penny, W. D. & Burgess, N. Brain oscillations and memory. *Curr. Opin.*  
306 *Neurobiol.* **20**, 143–149 (2010).

307 29. Stevenson, I. H., Rebisco, J. M., Miller, L. E. & Kording, K. P. Inferring functional  
308 connections between neurons. *Curr. Opin. Neurobiol.* **18**, 582–588 (2008).

309 30. Van Dijk, K. R. A. *et al.* Intrinsic Functional Connectivity As a Tool For Human  
310 Connectomics: Theory, Properties, and Optimization. *J. Neurophysiol.* **103**, 297–321  
311 (2010).

312 31. Buzsáki, G. & Draguhn, A. Neuronal Oscillations in Cortical Networks. *Science* (80-. ).  
313 **304**, (2004).

314 32. Jacobs, J., Kahana, M. J., Ekstrom, A. D. & Fried, I. Brain oscillations control timing of  
315 single-neuron activity in humans. *J. Neurosci.* **27**, 3839–44 (2007).

316 33. Schalk, G. A general framework for dynamic cortical function: the function-through-  
317 biased-oscillations (FBO) hypothesis. *Front. Hum. Neurosci.* **9**, 352 (2015).

318 34. Burke, J. F. *et al.* Human intracranial high-frequency activity during memory processing:  
319 neural oscillations or stochastic volatility? This review comes from a themed issue on  
320 Brain rhythms and dynamic coordination. *Curr. Opin. Neurobiol.* **31**, 104–110 (2015).

321 35. Fox, K. C. R., Foster, B. L., Kucyi, A., Daitch, A. L. & Parvizi, J. Intracranial  
322 Electrophysiology of the Human Default Network. *Trends Cogn. Sci.* **22**, 307–324 (2018).

323 36. Yushkevich, P. A. *et al.* Automated volumetry and regional thickness analysis of  
324 hippocampal subfields and medial temporal cortical structures in mild cognitive  
325 impairment. *Hum. Brain Mapp.* **36**, 258–87 (2015).

326 37. Avants, B. B., Epstein, C. L., Grossman, M. & Gee, J. C. Symmetric diffeomorphic image  
327 registration with cross-correlation: Evaluating automated labeling of elderly and  
328 neurodegenerative brain. *Med. Image Anal.* **12**, 26–41 (2008).

329 38. Gramfort, A. *et al.* MNE software for processing MEG and EEG data. *Neuroimage* **86**,  
330 446–460 (2014).

331 39. Scheeringa, R. *et al.* Neuronal Dynamics Underlying High- and Low-Frequency EEG  
332 Oscillations Contribute Independently to the Human BOLD Signal. *Neuron* **69**, 572–583  
333 (2011).

334 40. Khambhati, A. N. *et al.* Virtual Cortical Resection Reveals Push-Pull Network Control  
335 Preceding Seizure Evolution. *Neuron* **91**, 1170–1182 (2016).

336 41. Shannon, R. V. A model of safe levels for electrical stimulation. *IEEE Trans. Biomed.*  
337 *Eng.* **39**, 424–426 (1992).

338 42. Fischl, B. FreeSurfer. *Neuroimage* **62**, 774–781 (2012).

339 43. Bullmore, E. & Sporns, O. Complex brain networks: graph theoretical analysis of  
340 structural and functional systems. *Nat. Rev. Neurosci.* **10**, 186–98 (2009).

341  
342  
343

344 **Supplementary Information** is linked to the online version of the paper at [www.nature.com](http://www.nature.com).

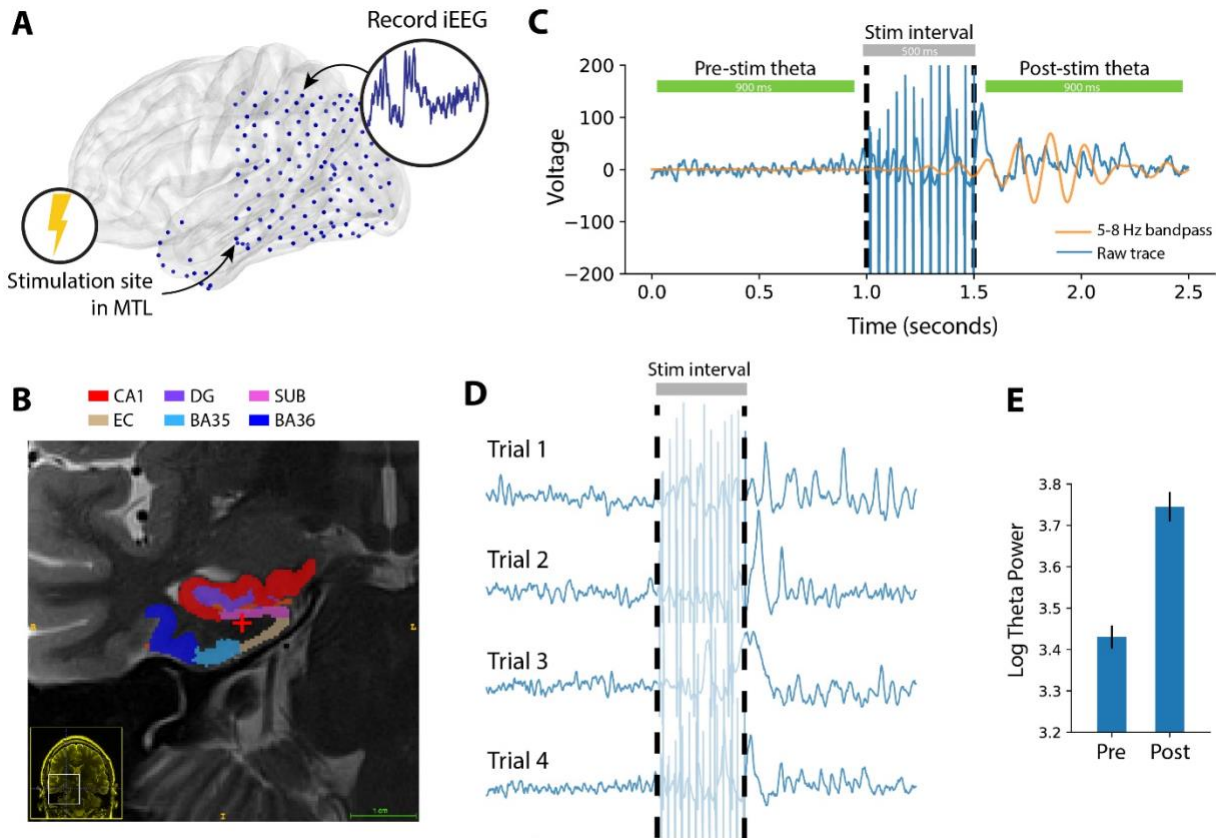
345 **Acknowledgements** We thank Blackrock Microsystems for providing neural recording equipment. This  
346 work was supported by the DARPA Restoring Active Memory (RAM) program (Cooperative Agreement  
347 N66001-14-2-4032), as well as National Institutes of Health grant MH55687 and T32NS091006. We are  
348 indebted to all patients who have selflessly volunteered their time to participate in our study. The views,  
349 opinions, and/or findings contained in this material are those of the authors and should not be interpreted  
350 as representing the official views or policies of the Department of Defense or the U.S. Government. We  
351 also thank Drs. Youssef Ezzyat, Christoph Weidemann, Nora Herweg, Danielle Bassett, and Geoffrey  
352 Aguirre for providing valuable feedback on this work.

353 **Author Contributions** E.S., M.J.K., and D.S.R. designed the study; E.S. conceived, planned, and  
354 executed all data analyses, J.K. analyzed data, and E.S. wrote the paper. J.S., R. Gorniak, S. Das.  
355 performed anatomical localization of depth electrodes. M.S., G.W., B.L., R. Gross., B.J., C.I., K.Z., S.  
356 Sheth, and S. Seger recruited subjects, collected data, and performed clinical duties associated with data  
357 collection including neurosurgical procedures or patient monitoring.

358 **Data Availability:** Raw electrophysiological data used in this study is freely available at  
359 [http://memory.psych.upenn.edu/Electrophysiological\\_Data](http://memory.psych.upenn.edu/Electrophysiological_Data)

360 **Competing Interests**

361 Michael J. Kahana and Daniel S. Rizzuto have started a company, Nia Therapeutics, LLC (“Nia”),  
362 intended to develop and commercialize brain stimulation therapies for memory restoration. Each of them  
363 holds more than 5% equity interest in Nia.



364  
365

366 **Figure 1. Comparison of pre- vs. post-stimulation theta (5-8 Hz) power in an example**

367 **subject.** (A) Each of 26 subjects received a series of 500 ms bipolar stimulation events, at 1-7  
368 sites within the MTL; an example subject schematic is shown here. (B) T2 MRI and MTL  
369 subregion segmentation for an example subject. Stimulation location, in white matter, is  
370 indicated at the red cross. See Supplemental Figure 1 for subregion labels. (C) Using the  
371 multitaper method, theta power (5-8 Hz) was measured in 900 ms windows preceding and  
372 following each stimulation event, with 50 ms buffers before and after stimulation. In an example  
373 stimulation event, the 5-8 Hz bandpass signal (orange) is overlaid on the raw bipolar signal  
374 (blue), to emphasize a change in pre- vs. post-stimulation theta power. (D) Theta power is  
375 extracted in the pre- and post-stimulation intervals for at least 240 events (“trials”) per

376 stimulation site. **(E)** The log-transformed theta power is aggregated for all pre- and post-  
377 stimulation intervals separately, for later statistical comparison (Fig. 2).

378

379

380

381

382

383

384

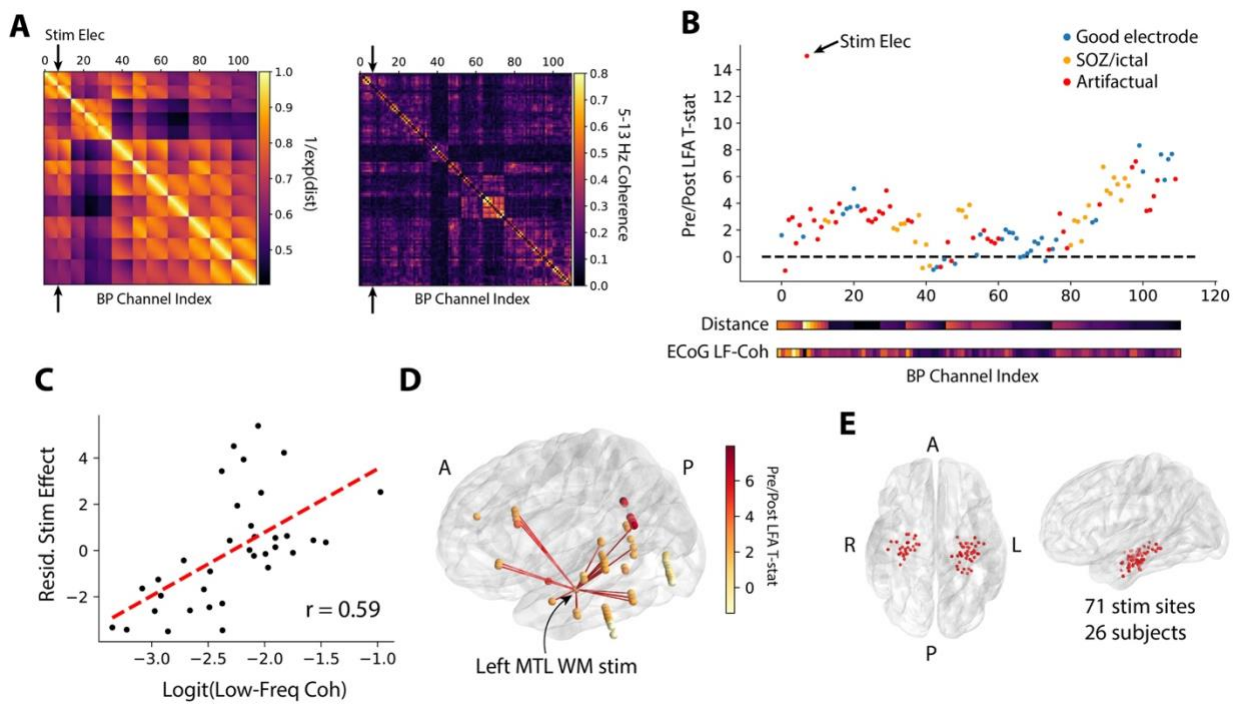
385

386

387

388

389

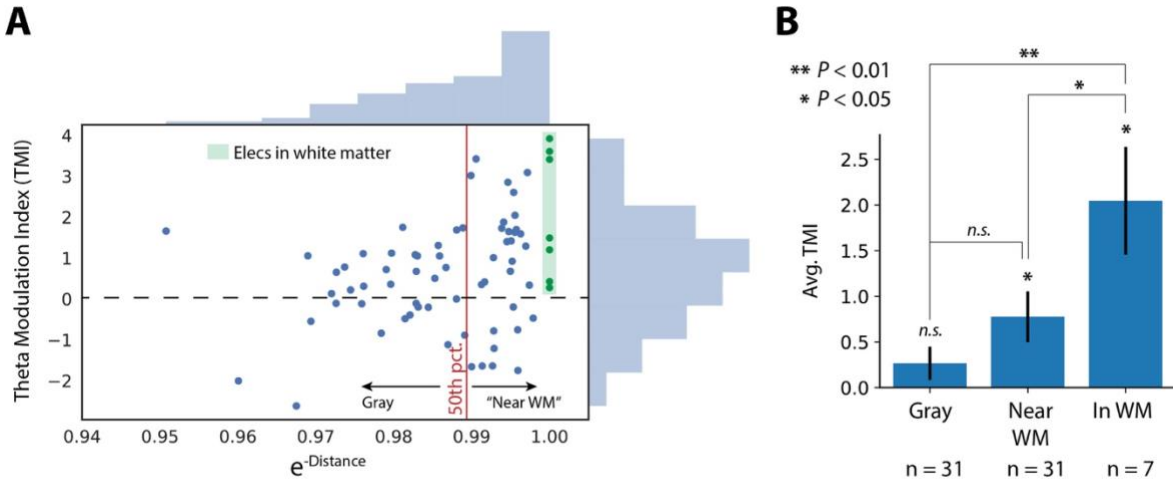


390  
391

**Figure 2. Method for determining theta modulation index (TMI).** (A) For each subject, 392 Euclidean distances (left matrix) and functional connectivity (right matrix) are measured for all 393 possible electrode pairs. Distances are linearized as  $e^{-(\text{distance})}$ , with 1.0 representing no separation 394 between two electrodes. Functional connectivity is the averaged 5-13 Hz multitaper coherence in 395 1-second windows extracted from a baseline period. (B) Pre- and post-stimulation theta power 396 (Fig. 1C) is compared with a paired t-test to generate a  $t$ -statistic for each electrode. Electrodes 397 are excluded from analysis if they exhibited significant post-stimulation artifact (red, see 398 Methods for details) or were placed in the seizure onset zone or exhibit high inter-ictal spiking 399 (orange). (C) Multiple linear regression is used to correlate the functional connectivity (between 400 a recording electrode and the stimulation electrode) with the power  $t$ -statistic, independent of 401 distance. To demonstrate this, the distance-residualized  $t$ -statistic (“Stim Effect”) is plotted 402 against functional connectivity in the example subject. The z-scored version of this correlation is 403 referred to as the “Theta Modulation Index,” or TMI. (D) Rendering of the power  $t$ -statistic as 404

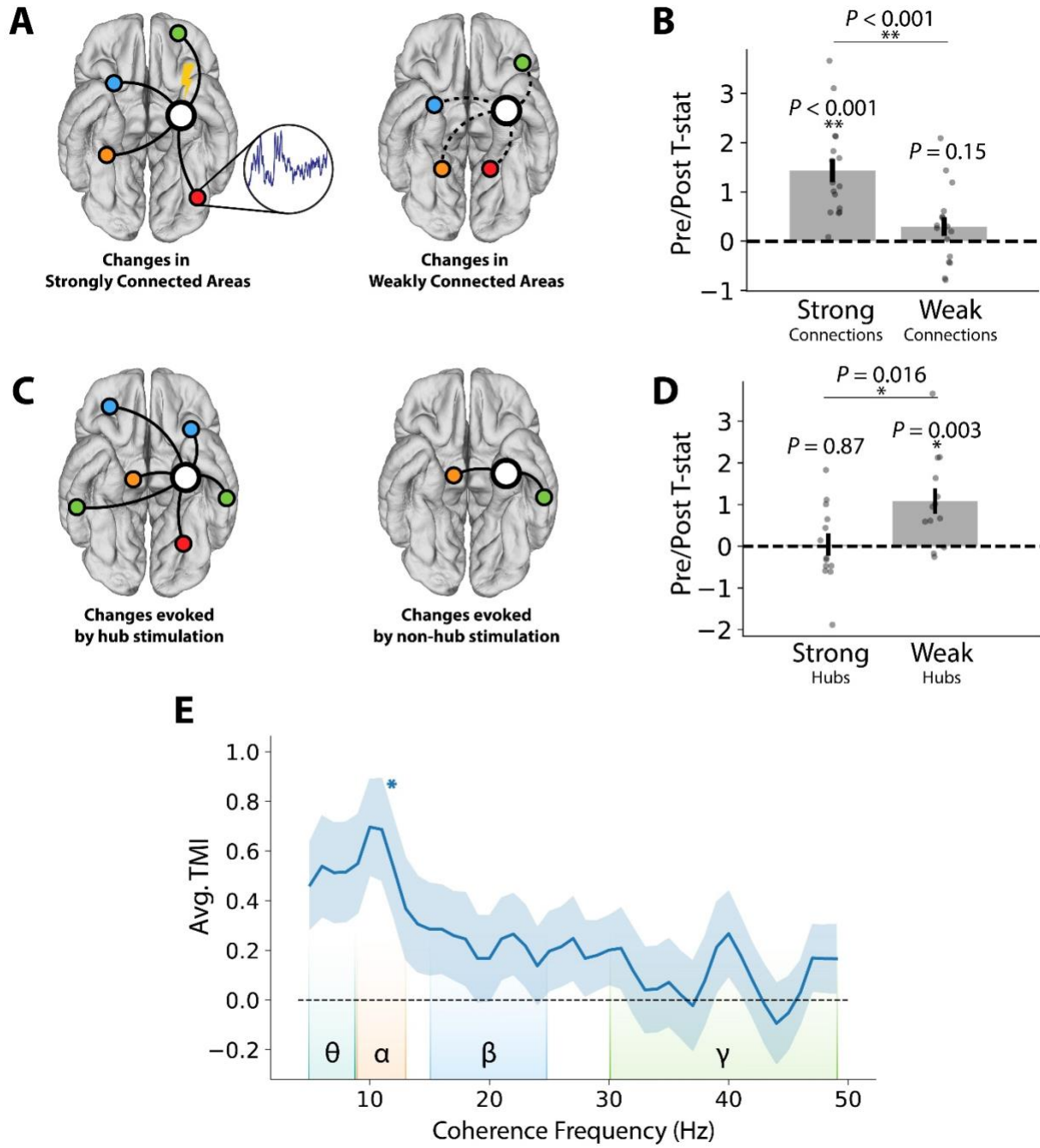
405 color on each electrode in the example subject, plotted with the top 10% of functional  
406 connections to the stim electrode (red lines). **(E)** Anatomical distribution of all MTL stimulation  
407 sites in the 26-subject dataset.

408  
409  
410  
411  
412  
413  
414  
415  
416  
417  
418  
419  
420  
421  
422  
423  
424  
425  
426  
427  
428  
429  
430  
431  
432  
433  
434  
435  
436



437  
438

439 **Figure 3. Proximity to white matter predicts TMI.** (A) Correlation between a stimulation  
440 site's distance from nearest white matter with the site's TMI. The 50<sup>th</sup> percentile of white matter  
441 distances divides sites classified as “gray matter” versus “near white matter.” Stimulated contacts  
442 in white matter are highlighted in green. See Supplemental Figure 2 for the Pearson correlation  
443 of these data ( $r = 0.33, P = 0.005$ ). (B) TMI increases with closeness to white matter, as  
444 determined by a permutation test ( $P < 0.001$ , see Methods) and by noting that TMIs for sites in  
445 or near white matter are significantly greater than zero (1-sample  $t$ -test,  $P < 0.05$ ) while gray  
446 matter sites are not ( $P = 0.15$ ). Electrodes placed in white matter have greater TMIs than  
447 electrodes near white matter (2-sample  $t$ -test,  $P < 0.05$ ) or gray matter ( $P < 0.01$ ). Error bars  
448 show +/- 1 SEM; \*  $P < 0.05$ ; \*\*  $P < 0.01$ .



449  
450

451 **Figure 4. Network properties of stimulation-induced theta.** (A) Schematic of a stimulation  
452 site and its most strongly-connected areas (left) or weakly-connected areas (right). (B) For each  
453 of 16 stimulation sites with significant TMI ( $P < 0.05$ ), the average post- vs. pre-stimulation  
454 theta T-statistic is computed for the five strongest-connected electrodes and the five weakest-  
455 connected electrodes (controlled for distance). Changes at strongly-connected recording sites are

456 significantly greater than changes at weakly-connected sites (paired *t*-test,  $t(15) = 6.03$ ,  $P = 1.7 \times$   
457  $10^{-5}$ ). **(C)** Schematic of a hub-like stimulation site (left) and a non-hub stimulation site (right).  
458 Hub scores are calculated as the node strength, or average of all connection weights to a given  
459 electrode. **(D)** For each of 40 stimulation sites in or near white matter, the average post- vs. pre-  
460 stimulation theta T-statistic is computed for the five strongest-connected recording electrodes.  
461 Stimulation of a weak hub (lower tercile of hub scores,  $n = 13$ ) yields significantly greater  
462 change in connected regions than stimulation of a strong hub (upper tercile of hub scores,  $n = 14$ )  
463 (2-sample *t*-test,  $P = 0.016$ ). **(E)** Average TMI across all in or near-white matter stimulation  
464 sites, as a function of functional connectivity frequency. TMI is greatest for networks  
465 constructed from theta or alpha coherence (5-13 Hz). Corrected for multiple comparisons across  
466 all frequencies, TMI is significantly greater than zero at 11 Hz. Error bars show  $\pm 1$  SEM; \*  $P$   
467  $< 0.05$ ; \*\*  $P < 0.001$ .

468  
469  
470  
471  
472  
473  
474  
475  
476  
477  
478  
479  
480  
481  
482  
483  
484  
485  
486  
487  
488  
489

490 **Methods**

491

492 Participants

493 Twenty-six patients with medication-resistant epilepsy underwent a surgical procedure to  
494 implant subdural platinum recording contacts on the cortical surface and within brain  
495 parenchyma. Contacts were placed so as to best localize epileptic regions. Data reported were  
496 collected at 8 hospitals over 4 years (2015-2018): Thomas Jefferson University Hospital  
497 (Philadelphia, PA), University of Texas Southwestern Medical Center (Dallas, TX), Emory  
498 University Hospital (Atlanta, GA), Dartmouth-Hitchcock Medical Center (Lebanon, NH),  
499 Hospital of the University of Pennsylvania (Philadelphia, PA), Mayo Clinic (Rochester, MN),  
500 National Institutes of Health (Bethesda, MD), and Columbia University Hospital (New York,  
501 NY). Prior to data collection, our research protocol was approved by the Institutional Review  
502 Board at participating hospitals, and informed consent was obtained from each participant.

503

504 Electrocorticographic recordings

505 iEEG signal was recorded using depth electrodes (contacts spaced 3.5-10 mm apart) using  
506 recording systems at each clinical site. iEEG systems included DeltaMed XITek (Natus), Grass  
507 Telefactor, and Nihon-Kohden EEG systems. Signals were sampled at 500, 1000, or 1600 Hz,  
508 depending on hardware restrictions and considerations of clinical application. Signals recorded at  
509 individual electrodes were first referenced to a common contact placed intracranially, on the  
510 scalp, or mastoid process. To eliminate potentially confounding large-scale artifacts and noise on  
511 the reference channel, we next re-referenced the data using a bipolar montage. Channels  
512 exhibiting highly non-physiologic signal due to damage or misplacement were excluded prior to  
513 re-referencing. The resulting bipolar timeseries was treated as a virtual electrode and used in all  
514 subsequent analysis.

515

516 Anatomical localization

517 To precisely localize MTL depth electrodes, hippocampal subfields and MTL cortices were  
518 automatically labeled in a pre-implant, T2-weighted MRI using the automatic segmentation of  
519 hippocampal subfields (ASHS) multi-atlas segmentation method <sup>36</sup>. Post-implant CT images  
520 were coregistered with presurgical T1 and T2 weighted structural scans with Advanced  
521 Normalization Tools <sup>37</sup>. MTL depth electrodes that were visible on CT scans were then localized  
522 within MTL subregions (including white matter) by neuroradiologists with expertise in MTL  
523 anatomy. All localizations in this manuscript refer to the bipolar midpoint of two recording  
524 contacts or the anode/cathode stimulation contacts.

525

526 Functional connectivity estimation

527 To obtain coherence values between electrode pairs, we used the MNE Python software package  
528 <sup>38</sup>, a collection of tools and processing pipelines for analyzing EEG data. The coherence ( $C_{xy}$ )  
529 between two signals is the normalized cross-spectral density (Equation 1); this can be thought of  
530 as the consistency of phase differences between signals at two electrodes, weighted by the  
531 correlated change in spectral power at both sites.

532

533 
$$C_{xy} = \left| \frac{S_{xy}}{S_{xx}S_{yy}} \right| \quad (1)$$

534 Where  $S_{xy}$  is the cross-spectral density between signals at electrodes  $x$  and  $y$ ;  $S_{xx}$  and  $S_{yy}$  are the  
535 auto-spectral densities at each electrode. Consistent with other studies of EEG coherence<sup>39,40</sup>, we  
536 used the multitaper method to estimate spectral density. We used a time-bandwidth product of 4  
537 and a maximum of 8 tapers (tapers with spectral energy less than 0.9 were removed), computing  
538 coherence for frequencies between 4-50 Hz, avoiding the 60 Hz frequency range that may be  
539 contaminated by line noise. Inter-electrode coherences were computed for a series of 1-second  
540 windows (minimum of 10 windows per subject) extracted from the baseline period of a non-  
541 stimulation task, in which subjects wait passively before beginning a verbal free-recall task. To  
542 construct the low-frequency networks used in the majority of this paper, cross-spectra were first  
543 averaged across all baseline period windows, normalized by the average power spectra, and then  
544 averaged between 5-13 Hz. For the analysis in Figure 4E, networks are constructed for each  
545 frequency between 4-50 Hz with no averaging over bands.

546

#### 547 Stimulation paradigm

548 At the start of each session, we determined the safe amplitude for stimulation using a mapping  
549 procedure in which stimulation was applied at 0.5 mA, while a neurologist monitored for  
550 afterdischarges. This procedure was repeated, incrementing the amplitude in steps of 0.5 mA, up  
551 to a maximum of 1.5 mA (chosen to be below the afterdischarge threshold and below accepted  
552 safety limits for charge density<sup>41</sup>). For each stimulation session, we passed electrical current  
553 through a single pair of adjacent electrode contacts in the MTL. Stimulation was delivered using  
554 charge-balanced biphasic rectangular pulses (pulse width = 300  $\mu$ s) at (10, 25, 50, 100, or 200)  
555 Hz frequency and (0.25 to 2.00) mA amplitude (0.25 mA steps) for 500 ms, with a minimum of 3  
556 seconds between stimulation events. During a session, subjects were instructed to sit quietly and  
557 did not perform any task. An average of 2.7 stimulation sites were selected for each subject, with  
558 a minimum of 240 trials delivered for each.

559

560 In most subjects, a post-stimulation voltage deflection artifact briefly contaminates a subset of  
561 recording contacts. To identify and remove channels exhibiting this artifact, the average voltage  
562 in the 350 ms prior to stimulation is compared with a paired t-test to the average voltage in the  
563 350 ms after stimulation, across all trials, for each channel. The same procedure is done with a  
564 levene test for different variances. Any electrode with a significantly different pre-vs.-post mean  
565 voltage or voltage variance ( $P < 0.01$ ) is excluded from further analysis (see “Estimating theta  
566 modulation index”). On average, this procedure excludes 28% of channels. Regardless of  
567 stimulation artifact, any bipolar pair is excluded from analysis if it shares a common contact with  
568 the stimulated pair.

569

#### 570 Spectral power analysis

571 We used the multitaper method to assess spectral power in the pre- and post-stimulation intervals  
572 (-950 to -50 ms relative to stimulation onset, and +50 to +950 ms after stimulation offset; Figure  
573 1B). We avoided the Morlet wavelet method to obviate the need for buffer periods that extend  
574 into the stimulation window. As in “Functional connectivity estimation,” we used the MNE  
575 Python software package. For each trial, theta power was taken as the average PSD from 5-8 Hz,  
576 using a time-bandwidth product of 4 and excluding tapers with < 90% spectral concentration. To  
577 compute a T-statistic at each electrode, the pre- vs. post log-transformed power values were  
578 compared with a paired t-test (Fig. 1D, Fig. 2B). We avoid calculating significances for

579 individual electrodes because sequential trials are non-independent events; T-statistics are only  
580 used for later correlation analysis (see “Theta modulation index”).  
581

#### 582 Estimating theta modulation index

583 To examine the relationship between stimulation and functional connectivity, we developed an  
584 index that reflects the correlation between theta power modulation and connectivity, independent  
585 of distance. To do this, we first construct low-frequency (5-13 Hz) networks as described in  
586 “Functional connectivity estimation,” and take the logit transform to linearize coherence values  
587 that fall between 0 and 1. We also construct adjacency matrices that reflect the normalized  
588 Euclidean distance between all possible pairs of electrodes (Fig. 2A), and linearize the distances  
589 by taking the reciprocal of their exponential (i.e. a Euclidean distance of zero would correspond  
590 to 1.0). For each stimulated electrode, we take that electrode’s distance and connectivity to all  
591 other electrodes as predictors of the theta power t-statistic (see “Spectral power analysis”) in a  
592 multiple linear regression. This controls for the effect of distance from a stimulation target,  
593 which is correlated with power and functional connectivity. Next, we permute the order of the  
594 predictors 1000 times and re-run the regression for each. The true coefficient for functional  
595 connectivity is compared to the distribution of null coefficients to obtain a z-score and p-value  
596 for each stimulation site. The z-score is referred to as the theta modulation index, or TMI.  
597

598 Prior to computing TMI, we excluded electrodes placed in the seizure onset zone or exhibiting  
599 significant inter-ictal spiking, as determined by a clinician. Electrodes with high post-stimulation  
600 artifact (see “Stimulation paradigm”), and stimulated electrodes themselves, were also excluded.  
601 Subjects were discarded if less than 10 electrodes remained after all exclusions.  
602

603 To analyze the relationship between TMI and white matter category (Fig. 3), we first binned  
604 electrodes according to their distance from nearest white matter. Distance were measured as the  
605 linearized Euclidean distance from a stimulation electrode (i.e. bipolar midpoint of the  
606 anode/cathode) to the nearest vertex of that subject’s Freesurfer white matter segmentation<sup>42</sup>  
607 based on T1 MRI. The 50<sup>th</sup> percentile of white matter distances marked the division between  
608 stimulation electrodes categorized as “near” white matter versus in gray matter. Seven  
609 stimulation electrodes were identified by expert neuroradiologists as being placed within white  
610 matter (see Supplementary Figure 2 for exact placements). To ask whether TMI increases with  
611 white matter category, permuted the white matter labels for each electrode 1000 times and took  
612 the minimum T-statistic between gray vs. near and near vs. in categories at each permutation. We  
613 then compared the minimum T-statistic in the true data to the distribution of null statistics to  
614 generate a p-value.  
615

#### 616 Network properties of stimulation

617 To determine how the network structure of a stimulation site affected downstream alterations in  
618 theta power (Fig. 4), we first analyzed the relationship between pre- vs. post-stimulation theta  
619 power and the strength of functional connectivity to a stimulation site (Fig. 4A-B). For each  
620 stimulation site with a significant TMI ( $P < 0.05$ ), we ranked all other electrodes by the strength  
621 of their functional connectivity to that site, residualized on Euclidean distance ( $e^{-dist}$ ). We then  
622 took the average power T-statistic (see “Spectral power analysis”) across the 5 strongest-  
623 connected sites and the 5 weakest-connected sites, to assess whether theta power changes  
624 correlated with the strength of a functional connection.

625  
626 To assess whether the effects of stimulation differ between hubs and non-hubs (Fig. 4C-D), we  
627 measured the node strength<sup>43</sup> for each stimulation site in or near white matter (n=38), using our  
628 low-frequency coherence networks (see “Functional connectivity estimation”). The node strength  
629 reflects the sum of all connection strengths to a given node (for this paper, we normalized node  
630 strength by the total number of possible connections for a given site, yielding strengths in the  
631 range from 0 to 1). For all stimulation sites, we binned hub scores by tercile, and took the highest  
632 tercile as “strong hubs,” the weakest tercile as “weak hubs” (n=13 for each). For stimulation at  
633 all strong and weak hubs, we took the average power T-statistic for the 5 strongest-connected  
634 electrodes. These values were used to assess whether hub stimulation tends to cause greater  
635 power changes in connected regions. The relationship between coherence frequency and theta  
636 modulation index (Figure 4E) was assessed by re-estimating the TMI (see “Estimating theta  
637 modulation index”) using spectral coherence networks observed for each frequency between 4-  
638 50 Hz, spaced by 1Hz, for all stimulation electrodes placed within or near white matter. The  
639 average TMI across sites/subjects was 1-sample *t*-tested against zero and p-values were FDR  
640 corrected for multiple comparisons (corrected  $P < 0.05$ ). For visualization purposes only, the  
641 displayed TMI/frequency curve was smoothed with a 3-point moving average window.